International Journal of Advances in Electrical Engineering

E-ISSN: 2708-4582
P-ISSN: 2708-4574
IJAEE 2023; 4(1): 69-77

www.electricaltechjournal.com
Received: 09-10-2022
Accepted: 16-12-2022

Crescent Onyebuchi OMEJE
Department of Electrical-Electronic Engineering, Faculty of Engineering, University of Port Harcourt, Choba, Port-Harcourt, Rivers State, Nigeria

Correspondence
Crescent Onyebuchi OMEJE
Department of Electrical-Electronic Engineering, Faculty of Engineering, University of Port Harcourt, Choba, Port-Harcourt, Rivers State, Nigeria

Modelling and evaluation of a resonant switched capacitor converter for a lithium-ion battery heating system of an automotive drive scheme

Crescent Onyebuchi OMEJE

Abstract
Lithium-ion battery forms an integral component in a hybrid electric vehicle. In a very cold climatic condition, it undergoes severe energy loss, poor performance and reduced life-cycle and therefore requires self-heating before starting. In this paper, a self-heating device that involves a resonant switched capacitor (RSC) heater with fast heating speed and high conversion efficiency was evaluated. The mathematical modeling and control of the RSC converter is presented. Simulation was carried out on the modelled equations and results obtained showed that the battery charging current significantly improved when the characteristic impedance of the model was increased. The RSC-heater conversion efficiency also increased to 91.05% at an increased characteristic impedance value of 4.5Ω All simulation processes were achieved in MATLAB/SIMULINK 2015 version.

Keywords: Hybrid electric vehicle (HEVs), lithium-ion (Li-ion) battery, resonant switched capacitor converter (RSC)

1. Introduction
Hybrid electric vehicles (HEV) have advanced swiftly in the recent technological progression due to the urgent need for energy conservation and immediate protection of the environment from fossil fuel pollution. A Lithium-ion battery forms an integral component in the operation of a hybrid electric vehicle and is adequately heated at a low temperature to avoid decrease in the discharge capacity thereby ensuring a stable operation.
Generally, in extreme cold climatic condition, the driving range of the HEV considerably drops due to the rapid increase in the internal resistance of the lithium-ion batteries which leads to a loss of usable energy [1, 2]. Lithium-ion batteries are conceived as the main power sources of HEV because of their inherent high energy density, no memory effect, low-self discharge rate and environmental friendliness [3]. However, in a chilly climate, Li-ion batteries undergo severe power decline and loss in energy which causes almost 40% - 50% decrease in HEV travelling speed range [4, 5]. To improve the battery performance and also increase the driving range of the HEV at low temperature, it is expedient that an effective on-board heating method be developed to preheat the battery to the desired temperature. In [6], Wang analyzed the battery preheating performance of plug-in hybrid electric vehicles and showed that the preheating could reduce the cost of PHEV operation by 22.3%. The various approaches that have been proposed for battery preheating at low temperatures are reported in [7 8].
In [9], Zhang proposed a low-frequency a.c heating approach which is based on external device. Though the a.c heating had little effect on the battery service life. In [10], Jiang built a high-accuracy and simple heating model for the a.c heating frequency which provided a guide in optimizing battery internal heating and charging strategies at low temperatures. In [11], Ruan *et al.* adopted an optimized heating frequency to maximize the temperature rise rate of the heating process without causing a detrimental effect on battery performance. In [12], ac-dc based self-heating approach was proposed to prevent Lithium-ion deposition. It was also verified that the proposed method caused little harm to the battery pack after a repeated heated tests. In [23], Guo *et al.* proposed an echelon pre-heating strategy to achieve a higher temperature rise rate for cold batteries. In [14], Wang *et al.* proposed a self-heating Lithium-ion battery with a new electrode that took few seconds to achieve almost 20-30 °C temperature rise with low energy loss. In [15], Zhang *et al.* tried to improve the self-heating performance of battery with almost 56% faster in heating speed and 24% less energy consumption through an embedded nickel foil heating element into the battery.

In [16, 17], an integral heater-equalizer was designed to realize the internal and external combined heating for cold batteries and also achieve a passive equalization for series connected battery strings. The reviewed work showed that with the same rms current, the increased a.c heating frequency would generate more electrochemical heat which helps to speed up the heating process. The existing battery power that is on-board heater based has two major drawbacks. The heaters work at hard switching method which leads to a high voltage stress on the MOSFETs, low reliability and high switching loss. Similarly, the a.c heaters generate triangular and sloped current of the same rms value which brings further potential damage to the batteries [18]. Battery self-heating at low temperatures requires high ac-heating frequencies. When a Lithium-ion battery is a.c heated, there is an exchange of the Lithium-ions between the cathode and the anode which continuously generates a large amount of heat inside the battery. The higher the a.c-heating frequency, the faster the Lithium-ions transport and more heat generated. Size and cost of a.c heater can be reduced at high a.c-heating frequencies which ensure easy implementation in HEV. Therefore, employing a resonant circuit formed by an inductor and a capacitor, the resonant switched capacitor (RSC) converters can easily generate a sinusoidal inductor current and capacitor voltage which provides a zero current condition for the switches conduction with reduced switching loss [19]. The various RSC topologies applied in the industry for battery self-heating are detailed in [20, 22].

This paper therefore focused on the modeling of the resonant switched capacitor converter heating current and its efficiency with pertinent to change in characteristic impedance. The variations in the quantity of heat in Joule dissipated by the battery self-resistance with respect to temperature difference are also presented. The discussed RSC self-heater exhibits superior features which include but not limited to compact size, low price, good reliability and high efficiency. This can be applied to battery systems of unmanned aerial vehicles and robots.

This paper is arranged in the following sequence: section 1: presents the introductory part of the work with some reviewed literature. Section 2: describes the RSC converter configuration for the Lithium-ion battery heating process. Section 3: mathematical modeling of the heating current and RSC converter efficiency with respect to the characteristic impedance and temperature variations were discussed. Section 4: simulation results are presented and discussed in this section. Section 5 concludes the core achievement of this paper.

2. RSC converter configuration for lithium-ion battery heating process

A resonant switched capacitor (RSC) heater for a battery module with N-cells connected in series is shown in Figure 1. It has one LC-circuit and two semi-conductor MOSFETS. The LC tank is connected in parallel with a MOSFET (Q_2). This parallel pair is further connected to the battery module through MOSFET (Q_1). To achieve the sinusoidal charging and discharging currents for the battery module, MOSFET Q_1 should have twice the duty cycle of Q_2 as shown in Figure 2.

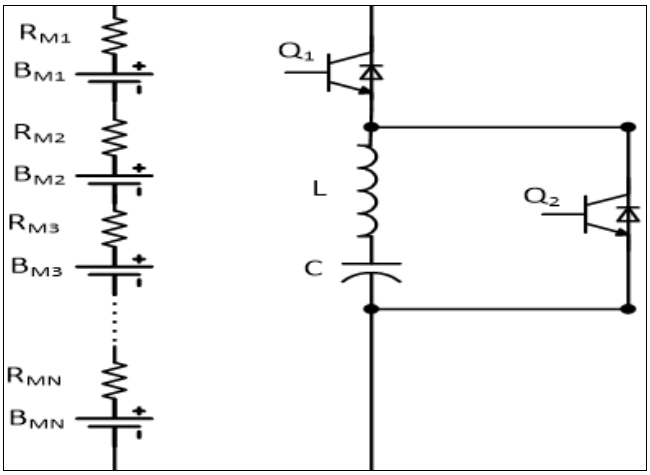

Fig 1: RSC-Heater Configuration for a battery module with N-cells.

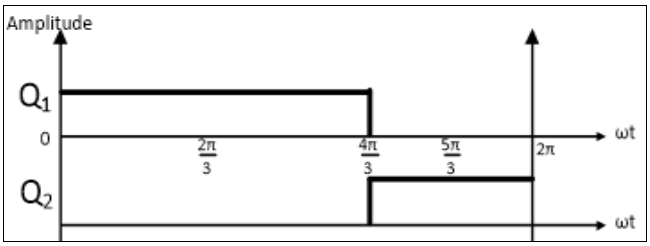

Fig 2: Firing Pulses of Q_1 and Q_2 signals

The operating states of the resonant switched capacitor heater presented in Figure 1 are illustrated as follows:

During the discharging state 1 when $0 \leq \omega t \leq \frac{2\pi}{3}$. Q_1 is switched on with zero-current switching while connecting the LC-tank in parallel with the battery module. The battery module is therefore discharged through the LC-tank.

During the charging state II when $\frac{2\pi}{3} < \omega t \leq \frac{4\pi}{3}$. Q_1 is still switched on and conduct for the span of $\frac{4\pi}{3}$. The battery module is therefore charged by the LC-tank.

During the balanced state III when $\frac{4\pi}{3} < \omega t \leq 2\pi$. Q_1 is switched off while Q_2 is turned on with zero-current switching (ZCS) while short-circuiting the LC tank. The capacitor is discharged and also reversely charged by the inductor. The three operating states are illustrated in Figures 3a,b,c with the active switching devices and current directions.

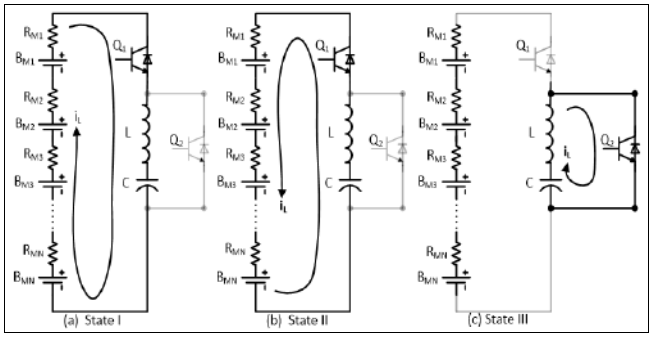

Fig 3: (a), (b) and (c): Operating States of the Resonant Switched Capacitor Converter

During a dead time between states III and I as shown in Figure 4(a), MOSFET Q_2 is turned off and the inductor current flows clockwise. It flows through the body diode of the MOSFET Q_1 and charges the battery module during this dead time. A zero voltage switching is achieved for Q_1 when it is turned on in state 1. As shown in Figure 4(b), when MOSFET Q_2 is turned off due to a changed direction in the inductor current, it is observed that current flows through the body diode of MOSFET Q_2 and charges the capacitor C during the dead time operation. Hence ZVS is realized for Q_2 when it is turned off in state III. This process makes the resonant switched operation robust and flexible to components tolerances and control.

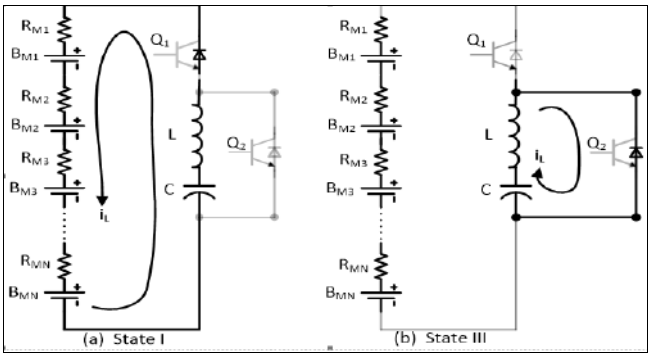

Fig 4: (a) and (b): Operating States of the RSC Converter during the dead time of Q_1 Q_2

3. Mathematical modelling of heating current and resonant switched capacitor (rsc) converter efficiency

Applying Kirchhoff's voltage law (KVL) in Figure 3a, the inductive current i_L and the capacitor voltage V_C during one switching period can be represented by equation (1).

$$\left.\begin{aligned} V_{oc} &= V_c + L\frac{di_L}{dt} + R.i_L \quad \text{for States I and II} \\ 0 &= V_c + L\frac{di_L}{dt} + R\,i_L \quad \text{for State III} \end{aligned}\right\} \tag{1}$$

Where V_{oc} = open circuit voltage of the battery module, R = equivalent resistance calculated from equation (2).

$$R = R_m + R_{LC} + R_{DS(on)} \tag{2}$$

R_m = Internal resistance of the battery module, R_{LC} = Equivalent resistance of the LC tank, $R_{DS\,(on)}$ = Drain-Source On-resistance of the MOSFET

Conventionally, the inductor current i_L and capacitor voltage V_c are related by equation (3).

$$i_L = C\frac{dV_c}{dt} \tag{3}$$

The time variation in current in terms of attenuation constant (α) and phase shift (β) is presented by equation (4)

$$i_{L(t)} = A\sin(\beta t)\, e^{\alpha t} \tag{4}$$

Where A = Amplitude of the inductor current, β = Phase Shift, and α = attenuation constant.

Substituting (4) into (1) for states I and II (charging and discharging states) gives rise to (5).

$$V_{oc} = V_C + L\frac{d}{dt}(A\sin(\beta t)\, e^{\alpha t}) + R\,(A\sin(\beta t)\, e^{\alpha t}) \tag{5}$$

$$\frac{d}{dt}(A\sin(\beta t)\, e^{\alpha t}) = A\alpha e^{\alpha t}\sin(\beta t) + A\beta e^{\alpha t}\cos(\beta t) \tag{6}$$

$$\alpha = \frac{-R}{2L} \tag{7}$$

Substituting (7) and (6) into (5) gives rise to the new open circuit voltage equation presented in (8).

$$V_{oc} = V_C + A\beta L e^{\alpha t}\cos(\beta t) + \frac{AR}{2} e^{\alpha t}\sin(\beta t) \tag{8}$$

The time varying capacitor voltage in terms of attenuation constant (α) and phase shift (β) is presented by (9).

$$V_{C(t)} = V_{oc} - A\beta L e^{\alpha t}\cos(\beta t) - \frac{AR}{2} e^{\alpha t}\sin(\beta t) \tag{9}$$

When $t = 0$ and $t = \frac{2\pi}{\beta}$. The amplitude of the capacitor voltage is obtained through a simultaneous solution of equation (9) for the different t-values and in accordance with references [36] and [37]. This gives rise to equation (10).

$$A = \frac{V_{oc}\left(1 + e^{\frac{\alpha}{\beta}\pi}\right)}{\beta L\left(1 + e^{\frac{3\alpha}{\beta}\pi}\right)} \tag{10}$$

Since $\beta = \sqrt{\frac{1}{LC} - \frac{R^2}{4L^2}}$, and characteristics impedance $Z = \sqrt{\frac{L}{C}}$, then the amplitude of the capacitor voltage in terms of the characteristics impedance is represented in equation (11).

$$A = \frac{V_{oc}\left(1 + e^{-\frac{\pi R}{2\sqrt{Z^2 - \frac{R^2}{4}}}}\right)}{\sqrt{Z^2 - \frac{R^2}{4}}\left(1 + e^{-\frac{3\pi R}{2\sqrt{Z^2 - \frac{R^2}{4}}}}\right)} \tag{11}$$

Substituting the expression of α β and A into equations (4) and (9) gives rise to equations (12) and (13).

$$i_{L(t)} = \frac{V_{oc}\left(1 + e^{-\frac{\pi R}{2\sqrt{Z^2 - \frac{R^2}{4}}}}\right)}{\sqrt{Z^2 - \frac{R^2}{4}}\left(1 + e^{-\frac{3\pi R}{2\sqrt{Z^2 - \frac{R^2}{4}}}}\right)} \sin\left(\sqrt{\frac{1}{LC} - \frac{R^2}{4L^2}}\,t\right) e^{\frac{-R}{2L}t} \tag{12}$$

$$V_{C(t)} = V_{oc}\,[\,1 - U\,[V]\, + W\,] + e^{-\frac{R}{2L}t} \quad (13)$$

$$U = \frac{(1 + e^{-\frac{\pi R}{2\sqrt{Z^2 - \frac{R^2}{4}}}})}{(1 + e^{-\frac{3\pi R}{2\sqrt{Z^2 - \frac{R^2}{4}}}})}$$

Where:

$$V = \cos\left(\sqrt{\frac{1}{LC} - \frac{R^2}{4L^2}}\,t\right), \quad W = \frac{R}{2\sqrt{Z^2 - \frac{R^2}{4}}} \sin\left(\sqrt{\frac{1}{LC} - \frac{R^2}{4L^2}}\,t\right)$$

It is observed that the amplitude of the heating current increases by reducing the characteristics impedance, reducing the equivalent resistance and also by increasing the open-circuit voltage.

Similarly, the inductor current and capacitor voltage during state III (balancing state) is derived through the same process and presented in equations (14) and (15).

$$i_{L(t)} = \frac{V_{oc}(e^{-\frac{\pi R}{\sqrt{Z^2 - \frac{R^2}{4}}}} - 1)}{\sqrt{Z^2 - \frac{R^2}{4}}(1 + e^{-\frac{3\pi R}{2\sqrt{Z^2 - \frac{R^2}{4}}}})} \sin\left(\sqrt{\frac{1}{LC} - \frac{R^2}{4L^2}}\,t - 2\pi\right) e^{\frac{-R}{2L}\left(t - \frac{2\pi}{\sqrt{\frac{1}{LC} - \frac{R^2}{4L^2}}}\right)} \quad (14)$$

$$V_{C(t)} = \frac{-V_{oc}(e^{-\frac{\pi R}{\sqrt{Z^2 - \frac{R^2}{4}}}} - 1)}{(1 + e^{-\frac{3\pi R}{2\sqrt{Z^2 - \frac{R^2}{4}}}})} [X + Y]\, e^{\frac{-R}{2L}\left(t - \frac{2\pi}{\sqrt{\frac{1}{LC} - \frac{R^2}{4L^2}}}\right)} \quad (15)$$

Where:

$$X = \mathrm{Cos}\left(\sqrt{\frac{1}{LC} - \frac{R^2}{4L^2}}\,t - 2\pi\right)$$

and

$$Y = \frac{R}{2\sqrt{Z^2 - \frac{R^2}{4}}} \sin\left(\sqrt{\frac{1}{LC} - \frac{R^2}{4L^2}}\,t - 2\pi\right).$$

The average discharging current of the battery module within one switching period is derived from equation (16).

$$I_{disch(avg)} = \frac{\int_0^{\frac{\pi}{\beta}} i_{L(t)}\,dt}{\frac{3\pi}{\beta}} = \frac{V_{oc}(e^{-\frac{\pi R}{2\sqrt{Z^2 - \frac{R^2}{4}}}} + 1)^2}{3\pi\sqrt{Z^2 - \frac{R^2}{4}}(1 + e^{-\frac{3\pi R}{2\sqrt{Z^2 - \frac{R^2}{4}}}})} \quad (16)$$

In like manner, the average charging current within one switching period is obtained from (17)

$$I_{ch(avg)} = \frac{\int_{\pi}^{\frac{2\pi}{\beta}} i_{L(t)}\,dt}{\frac{3\pi}{\beta}} = \frac{-V_{oc}(e^{-\frac{\pi R}{2\sqrt{Z^2 - \frac{R^2}{4}}}})(e^{-\frac{\pi R}{2\sqrt{Z^2 - \frac{R^2}{4}}}} + 1)^2}{3\pi\sqrt{Z^2 - \frac{R^2}{4}}(1 + e^{-\frac{3\pi R}{2\sqrt{Z^2 - \frac{R^2}{4}}}})} \quad (17)$$

The efficiency of the Resonant Switched Capacitor converter is determined from equation (18)

$$\eta_c = \left|\frac{I_{ch(avg)}(V_{oc} - I_{ch(avg)}R_M)}{I_{dis(avg)}(V_{oc} - I_{dis(avg)}R_M)}\right| \cong e^{-\left(\frac{\pi(R_{LC} + R_{DS(on)})}{2\sqrt{Z^2 - \frac{(R_{LC} - R_{DS(on)})^2}{4}}}\right)} \quad (18)$$

It is obvious that the conversion efficiency is improved by increasing the characteristic impedance Z which results to a small heating current. To enhance the conversion efficiency and heating current, a small equivalent resistance of the LC tank (R_{LC}) and Drain-Source on-resistance ($R_{DS(on)}$) are applied since the ac heating mainly depends on the battery Ohmic loss. Therefore, the heating efficiency for the battery modules is presented in equation (19).

$$\eta_h = \frac{I_L^2 R_M}{I_L^2 (R_M + R_{LC} + R_{DS(on)})} = \frac{R_M}{(R_M + R_{LC} + R_{DS(on)})} \times 100 \quad (19)$$

Where: I_L = rms heating current. It is apparent that a larger internal resistance R_M, smaller equivalent resistance of the LC tank R_{LC} and smaller drain-source on-resistance of the MOSFET will produce a higher heating efficiency which implies more useful power for batteries heating.

Temperature measurements of Li-ion batteries are important for supporting Battery Management Systems in controlling highly relevant states, such as State-of-Charge and State-of-Health. In addition, temperature measurements are essential in preventing dangerous situations and also in maximizing the performance and life cycle of batteries. However, due to thermal gradients, which might quickly develop during operation, fast and accurate temperature measurements can be rather challenging. For a proper selection of the temperature measurement method, aspects such as measurement range, accuracy, resolution, and costs of the methods are important. At present, traditional temperature measurement methods, such as thermistors and thermocouples, are extensively used. Several recently introduced methods, such as impedance-based temperature indication and fiber Bragg-grating techniques, are under investigation in order to determine their suitability for large scale introduction in sophisticated battery-powered applications. When a battery operates in a humid environment, there is a convectional heat exchange between

the surface and the surroundings. In addition, the battery surface is cooled down by emitting infrared radiation. Heat exchanges by convection ($Q_{Conv.}$) and radiation ($Q_{Rad.}$) with the drive environment are represented by equations (20) and (22).

$$Q_{Conv.} = hA(T - T_a) \quad (20)$$

$$Q_{Rad.} = \sigma\varepsilon A(T^4 - T_a^4) \quad (22)$$

Where: h = heat-transfer coefficient (W/m^2K), A = surface area of the battery, T=battery surface temperature (K), T_a = ambient temperature (K), σ = Stefan-Boltzmann constant (W/m^2K^4) = 5.6×10^{-8} and ε = emissivity ($0 < \varepsilon \leq 1$) of the surface material. Heat dissipation from battery to the environment is given by equation (4).

$$Q_{out.} = Q_{Conv.} + Q_{Rad.} = hA(T - T_a) + \sigma\varepsilon A(T^4 - T_a^4) \quad (22)$$

4. Simulation results and discussions

Simulation was achieved with the parameters presented in Table 1. Figure 5 shows the characteristic waveform of the charging and discharging current at varying characteristic impedance. It is observed that at a very large characteristic impedance, the discharging current decreases while the charging current rises in accordance with equations (16) and (17). When the characteristic impedance gets to a value of 400Ω, the charging and discharging current attains a stable and constant state value of 0.03959 A and -0.03922 A.

Figure 6 depicts the converter efficiency against the characteristic impedance and battery heat dissipation with temperature change. It is observed that the efficiency rises with a corresponding increase in the characteristic impedance attaining a steady state value of 91.05% at 4.5Ω. Similarly, the heat dissipation varied linearly with the temperature change. It is also observed that at a very low temperature value more heat is required by the RSC converter in self-heating the Lithium-ion battery to a charged state. A plot of the firing pulses for the MOSFETS Q_1 and Q_2 is presented in Figure 7. It clearly shows that the duty cycle of the PWM for Q_1 is high above 50% of the PWM for Q_2 and both conduct in a complementary mode.

Figure 8 represents the plot of inductor current and capacitor voltage. It is observed that the inductor current is a pure sinusoidal wave which ensured reduced harmonics and excess heat losses associated with a distorted triangular waveform for battery self-heating. In like manner, the capacitor voltage ensured a zero voltage switching which is applied in the controlled regulation of the Q_1 and Q_2 conduction.

Figure 9 shows the variation in RSC-AC voltage and battery charging current with time. It is obvious from the waveforms that with an elapse in time, the magnitude of the resonant switched capacitor ac voltage depreciated and as a consequence affects the amplitude of the charging current with time. This phenomenon is the major disadvantage that is associated with a battery operated hybrid electric vehicle for a long distance speed racing.

Table 1: Simulation Parameters of the Resonant Switched Capacitor Converter.

Parameters	Values	Symbol
Ambient temperature (°C)	25	Ta
Battery temperature (°C)	0:5:50	T
Heat transfer coefficient (W/m^2K)	0.5	h
Battery surface area (m^2)	0.012	A
Emissivity of the surface material	0.5	ε
Stefan-Boltzmann Constant (W/m^2K^4)	$5.67x10^{-8}$	σ
Battery Capacity (mAh)	2500	C_B
Open circuit voltage (V)	30.6	Voc
Capacitance (μF)	475	C
Inductance (mH)	25	L
Equivalent Resistance of the LC tank (mΩ)	15	RLC
Battery internal resistance at 0°C (mΩ)	180	RM
Drain-Source on-resistance of MOSFET (mΩ)	240	RDS(on)
MOSFET switching frequency (Hz)	5000	F_S

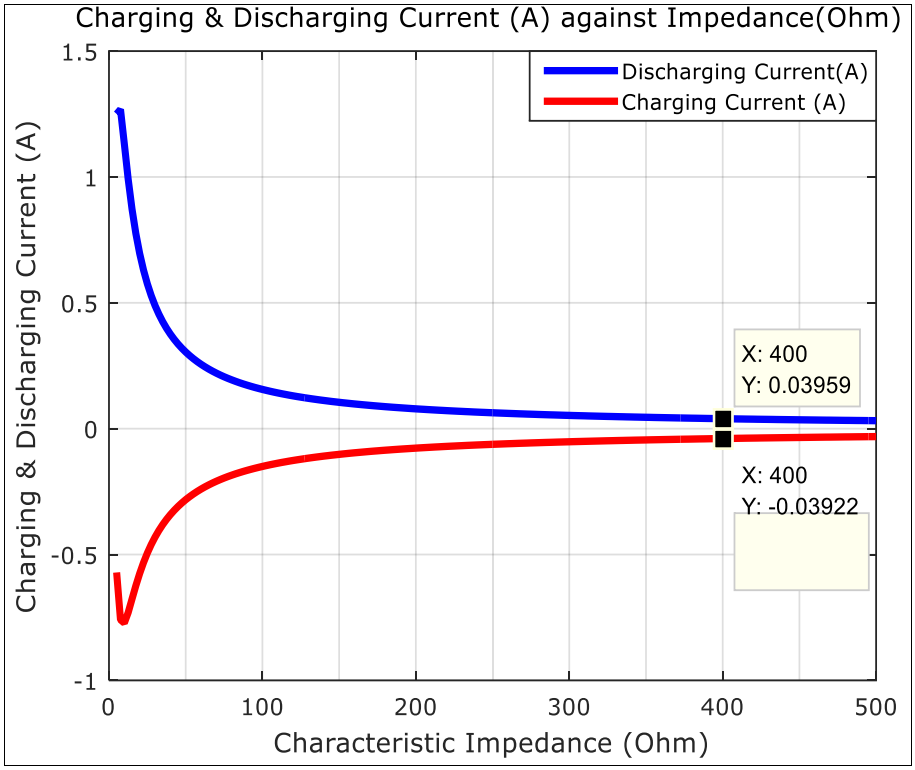

Fig 5: $I_{ch(avg)}$ & $I_{disch(avg)}$ against Impedance

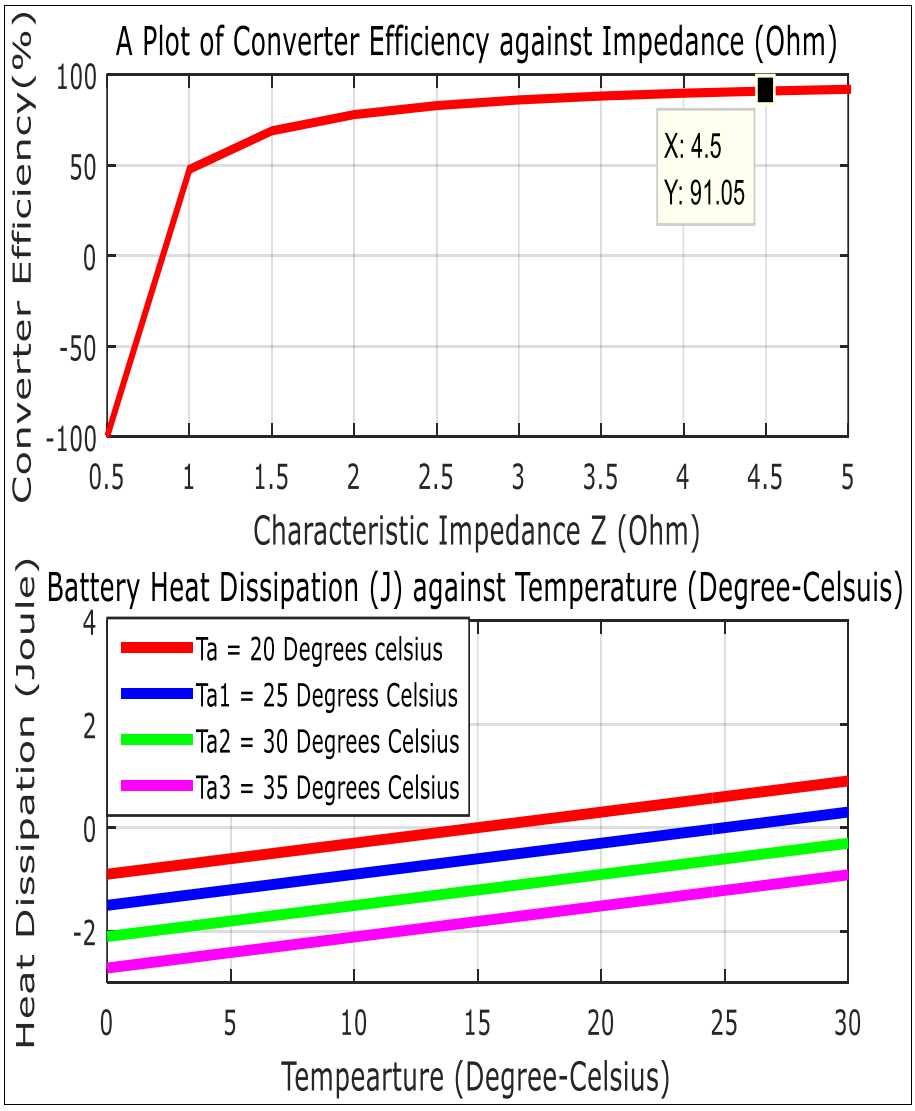

Fig 6: Efficiency against Impedance & Heat against Temp.

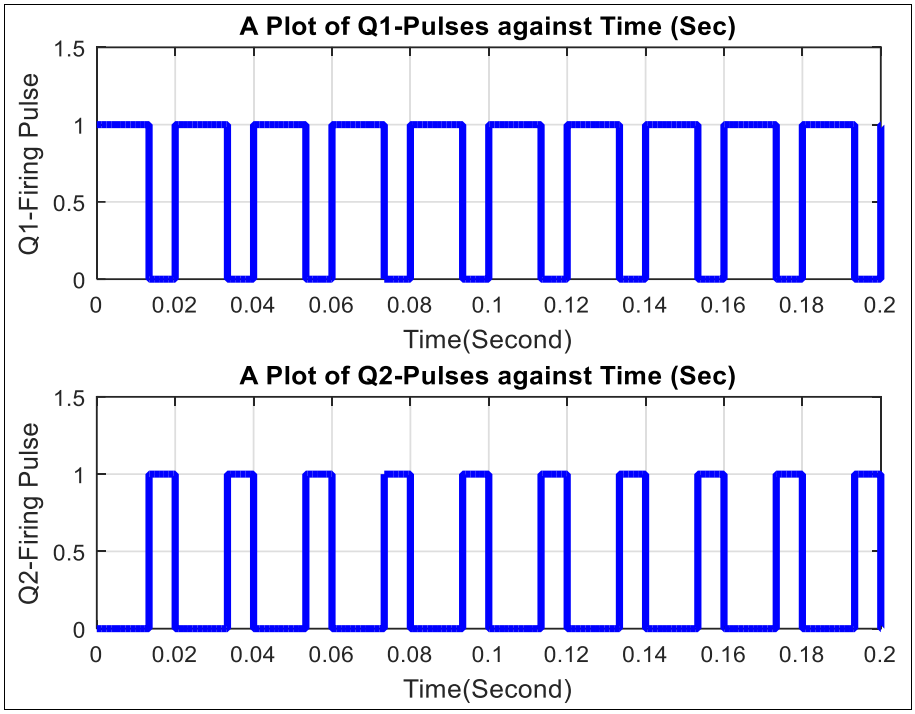

Fig 7: Firing Pulses for Mosfets Q1 and Q2 Signals.

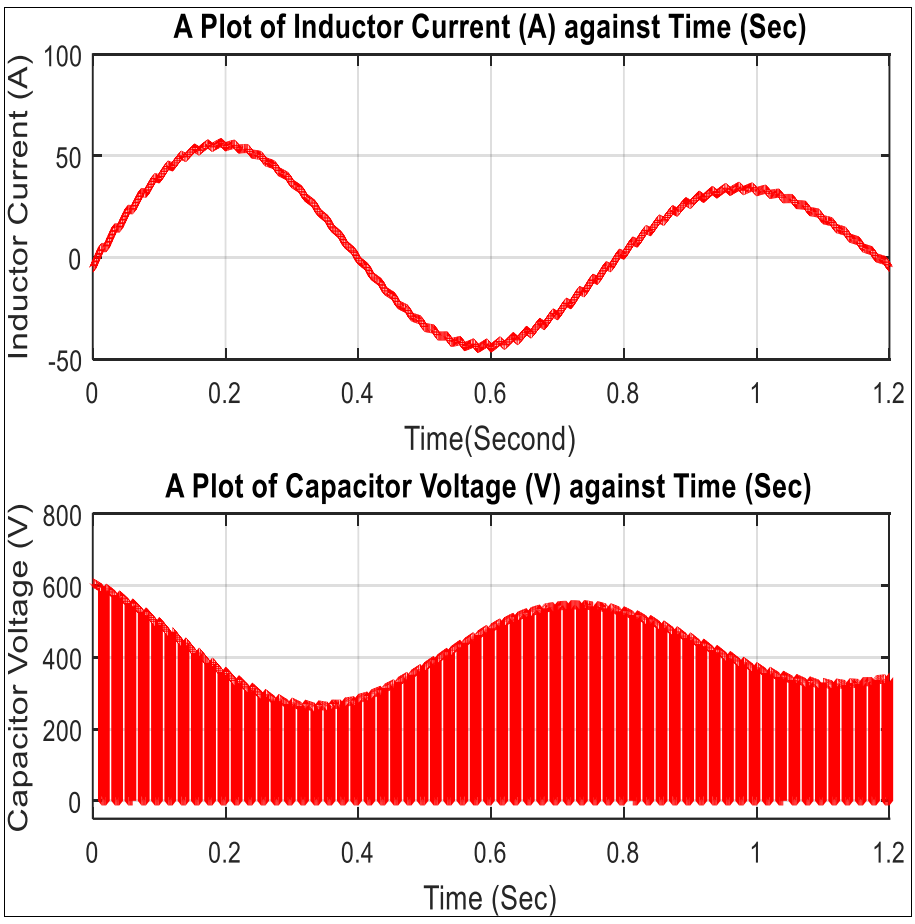

Fig 8: Inductor current & capacitor voltage against

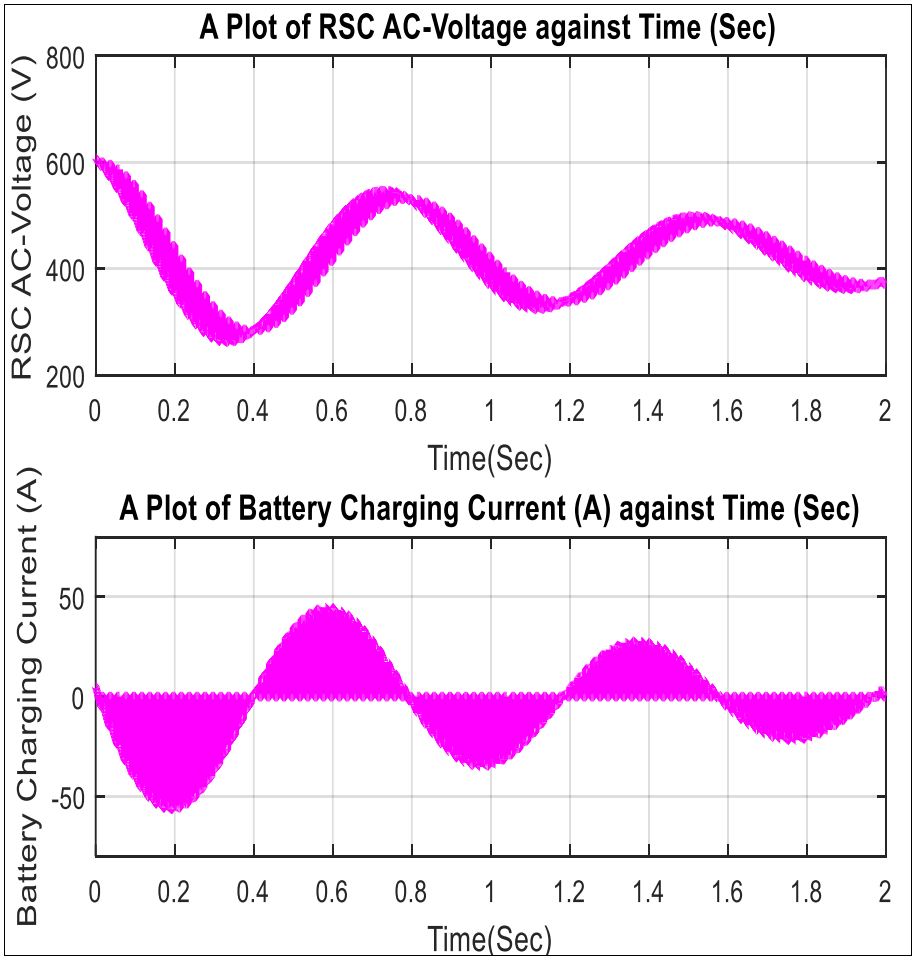

Fig 9: RSC voltage & charging current against Time.

5. Conclusion

This paper has illustrated the dynamic performance of the resonant switched capacitor converter (RSC) with ac heating capability for Lithium-ion battery applied in hybrid electrics vehicle (HEV). The detailed operation and mathematical modeling for the ac current were carried out. A sine-wave for the battery pack heating without the involvement of external power source was realized. The battery charging current was significantly improved by increasing the characteristic impedance leading to high conversion efficiency with a decreased magnitude in the discharging current. Therefore, with a suitable choice of characteristic impedance, the RSC heater can be readily applied in preheating the batteries in various applications such as unmanned aerial vehicles and robotics.

It is recommended that the heat generated by the MOSFET as a result of switching loss and diode conduction loss be utilized in the external heating of the batteries to further improve the heating speed and conversion efficiency especially for a long distance speed racing electric vehicles.

6. References.

1. Liu K, Li K, Peng Q, Zhang C. A brief review on key technologies in the battery management system of electric vehicles, frontiers in Mech. Eng. 2019 Nov;14(1):47-64.
2. Kellar A, Dasari Y, Williamson SS. A comprehensive review of power electronics enabled active battery cell balancing for smart energy management, In 2020 IEEE International conference on Power electronics, smart grid and renewable energy (PESGRE 2020) Cochin, India; c2020. p. 1-6.
3. Ding X. A novel active equalization topology for series-connected Lithium-ion battery packs. IEEE. Trans. Ind. Appl. 2020;56(6):6892-6903.
4. Kim DH, Kim MJ, Lee BK. an Integrated battery charger with high power density and efficiency for electric vehicles," IEEE Trans. Power Electron. 2017 Jan;32(6):4553-4565.
5. Mohan S, Kim Y, Stephanopoulos AG. Energy conscious warm-up of Li-ion cells from subzero temperatures, IEEE Trans. Ind. Electron. 2016;63(5):2954-2964.
6. Wang T. Performance of plug-in hybrid electric vehicle under low temperature condition and economy analysis of battery pre-heating, Journal of Power Sources. 2018 Sept;401:245-254.
7. Jiang J. A low temperature internal heating strategy without life-time reduction for large-size automotive Lithium-ion battery pack, Appl. Energy. 2018 Aug;230:257-266.
8. Yiang X, Liu T, Wang C. Innovative heating of large size automotive Li-ion cells, Journal of Power Sources. 2017 Feb;342:598-604.
9. Zhang J, Gee H, Li Z, Ding Z. Internal heating of Lithium-ion batteries using alternating current based on the heat generation model in frequency domain, Journal of Power Sources. 2015 Jan;273:1030-1037.
10. Jiang J. A reduced low-temperature electro-thermal coupled model for Lithium-ion batteries, Appl. Energy. 2016 Sep;177:804-816.
11. Ruan H. A rapid low-temperature internal heating

strategy with optimal frequency based on constant polarization voltage for Lithium-ion batteries, Appl. Energy. 2016 Sep;177:771-782.
12. Shang Y, Xiu B, Cui N, Zhang C, Mi C. An automotive On-board AC-heater without external power supplies for Lithium-ion batteries at low temperature, IEEE. Trans. Power Electron. 2017 Nov;33(9):7759-7769.
13. Singh J. Mathematical modeling with mixed chemotherapy on tumor cells in two different stages under depression effect. Int. J. Stat. Appl. Math. 2021;6(1):242-248.
DOI: 10.22271/maths.2021.v6.i1c.655
14. Wang C. Lithium-ion battery structure that self-heats at low temperatures. Nature. 2016 Jan;529(7587):515-518.
15. Zhang G, Gr S, Xu T, Yang XG, Tian H, Wang CY. Rapid self-heating and internal temperature sensing of Lithium-ion batteries at low temperatures, Electrochem. Acta. 2016;218:149-155.
16. Shang Y, Zhu C, Fu Y, Mi C. An integrated heater – equalizer for Lithium-ion batteries of electric vehicles, IEEE Trans. Ind. Electron. 2019 Jan;66(6):4398-4405.
17. Shang Y, Zhang Q, Cui N, Zhang C. A cell-to-cell equalizer based on three resonant state switched capacitor converters for series-connected battery strings, Energies. 2017 Feb;10(206):1-5.
18. Yang Y, Wei X, Liu Y, Dai H, Zhu J, Fang Q. A research on the ac heating of automotive Lithium-ion battery, Automotiv. Eng. 2016 Jul;38(7):901-908.
19. Cervera A, Mordechai-Peretz M. Resonant switched capacitor voltage regulator with ideal transient response, IEEE Trans. Power Electron. 2015 Sep;30(9):4943-4951.
20. Li S, Zheng Y, Wu B, Smedley KM. A family of resonant two switch boosting switched capacitor converter with ZVS operation and a wide line regulation range, IEEE Trans. Power Electron. 2018 Jan;33(1):448-459.
21. Cervera A, Evzelman M, Mordecai,-Peretz M, Ben-Yaakov S. A high efficiency resonant switched capacitor converter with continuous conversion ratio, IEEE-Trans. Power Electron. 2015 Mar;30(3):1373-1382.
22. Li S, Xiangli K, Zheng Y, Smedley KM. Analysis and design of the ladder resonant switched capacitor converters for regulated output voltage application, IEEE Trans. Ind. Electron. 2017 Oct;64(10):7769-7779.
23. Guo S, Xiong R, Wang K, Sun F. A novel echelon internal heating strategy of cold batteries for all climate electric vehicles application, Appl. Energy. 2018;219:256-263.